

Coping with uncertainties through an automated workflow for 3D reservoir modelling of carbonate reservoirs

*Original*

Coping with uncertainties through an automated workflow for 3D reservoir modelling of carbonate reservoirs / Benetatos, Christoforos; Giglio, Giorgio. - In: GEOSCIENCE FRONTIERS. - ISSN 1674-9871. - ELETTRONICO. - 12:(2021). [10.1016/j.gsf.2019.11.008]

*Availability:*

This version is available at: 11583/2780253 since: 2023-05-21T10:03:54Z

*Publisher:*

Elsevier

*Published*

DOI:10.1016/j.gsf.2019.11.008

*Terms of use:*

This article is made available under terms and conditions as specified in the corresponding bibliographic description in the repository

*Publisher copyright*

(Article begins on next page)

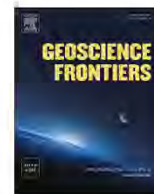
HOSTED BY



ELSEVIER

Contents lists available at ScienceDirect

Geoscience Frontiers

journal homepage: [www.elsevier.com/locate/gsf](http://www.elsevier.com/locate/gsf)

# Coping with uncertainties through an automated workflow for 3D reservoir modelling of carbonate reservoirs

Christoforos Benetatos<sup>a,\*</sup>, Giorgio Giglio<sup>b</sup>

<sup>a</sup> Department of Environment, Land and Infrastructure Engineering, Politecnico di Torino, Corso Duca Degli Abruzzi 24, 10129, Torino, Italy

<sup>b</sup> DREAM Srl, Via Asinari di Bernezzo 67, 10146, Torino, Italy

## ARTICLE INFO

### Keywords:

Uncertainty propagation  
3D geological modelling  
Integrated study  
Carbonate rock  
Risk analysis

## ABSTRACT

Reliable 3D modelling of underground hydrocarbon reservoirs is a challenging task due to the complexity of the underground geological formations and to the availability of different types of data that are typically affected by uncertainties. In the case of geologically complex depositional environments, such as fractured hydrocarbon reservoirs, the uncertainties involved in the modelling process demand accurate analysis and quantification in order to provide a reliable confidence range of volumetric estimations. In the present work, we used a 3D model of a fractured carbonate reservoir and populated it with different lithological and petrophysical properties. The available dataset also included a discrete fracture network (DFN) property that was used to model the fracture distribution. Uncertainties affecting lithological facies, their geometry and absolute positions (related to the fault system), fracture distribution and petrophysical properties were accounted for. We included all different types of uncertainties in an automated approach using tools available in today's modelling software packages and combining all the uncertain input parameters in a series of statistically representative geological realizations. In particular, we defined a specific workflow for the definition of the absolute permeability according to an equivalent, single porosity approach, taking into account the contribution of both the matrix and the fracture system. The results of the analyses were transferred into a 3D numerical fluid-dynamic simulator to evaluate the propagation of the uncertainties associated to the input data down to the final results, and to assess the dynamic response of the reservoir following a selected development plan. The "integrated approach" presented in this paper can be useful for all technicians involved in the construction and validation of 3D numerical models of hydrocarbon-bearing reservoirs and can potentially become part of the educational training for young geoscientists and engineers, since an integrated and well-constructed workflow is the backbone of any reservoir study.

## 1. Introduction

A reservoir model incorporates different types of data (geological, petrophysical, geophysical, pressure profiles, production history if any) that is characterized by different scales, resolutions and associated uncertainties. Successful use of these assorted datasets to constrain a reservoir model is strongly linked to the modelling approach. Over the last decades, integrated approaches (Cosentino, 2001; Worthington and Cosentino, 2005; Benetatos and Viberti, 2010; Le Laverac et al., 2014; Moscarriello, 2016 and references therein) have proved valuable in constructing reliable 3D models that can capture the geological and dynamic features of a reservoir and that are able to accurately describe the

interactions occurring among wells, rocks and fluids. This is possible via a multidisciplinary methodology that can guarantee a continuous improvement of the model through subsequent steps and hence delivery of a geologically accurate and dynamically functional reservoir model. In fact, the most widespread industry software packages now provide a common platform for geophysicists, geologists and engineers to work together; such a platform has improved data handling and decision making, leading to more coherent reservoir representations.

Even though important steps were made towards a fully integrated approach in reservoir modelling (e.g. Al Qassad et al., 2000; Ouenes and Hartley, 2000; Du et al., 2009; Cipolla et al., 2010; Ma et al., 2011; Senel et al., 2014), the quality of the results remains strongly dependent on the

\* Corresponding author.

E-mail addresses: [christoforos.benetatos@polito.it](mailto:christoforos.benetatos@polito.it), [giorgio.giglio@dream-top.com](mailto:giorgio.giglio@dream-top.com) (C. Benetatos).

Peer-review under responsibility of China University of Geosciences (Beijing).

<https://doi.org/10.1016/j.gsf.2019.11.008>

Received 10 October 2019; Received in revised form 30 October 2019; Accepted 16 November 2019

Available online xxxx

1674-9871/© 2019 China University of Geosciences (Beijing) and Peking University. Production and hosting by Elsevier B.V. This is an open access article under the

CC BY-NC-ND license (<http://creativecommons.org/licenses/by-nc-nd/4.0/>).

quality of the input data (abundance, reservoir coverage, uncertainty ranges, etc.). Accurate handling of the uncertainties associated with the various modelling parameters and their integration into the 3D model can provide an estimation of a reliable range of the volume of hydrocarbon in place and, ultimately, of the recoverable reserves and final recovery factor through dynamic simulations.

In the present work, we focus on the uncertainties associated with geophysical, geological and petrophysical data and their impact on the distribution of facies and petrophysical parameters, on how they propagate to the volume of hydrocarbon in place but also on how they affect the outcome of dynamic simulations. We will show how different types of uncertainties can be handled in an automated approach using tools available in today's modelling software packages. To this end, we used the case of a fractured carbonate reservoir and we generated the reservoir model integrating a variety of depositional and geological uncertainties into the analysis, such as commonly encountered uncertainties linked to facies geometrical relations, lithological and petrophysical values variations. In addition, we combined the contribution of core-derived matrix permeability with a fracture intensity attribute map defined in the discrete fracture network model in order to calculate an equivalent absolute permeability incorporating the contribution of both the matrix and the fracture systems.

## 2. Static modelling workflow

In a reservoir study the "traditional" static modelling workflow (e.g. Labourdette et al., 2008; Shao et al., 2011 and references therein) implies following a series of basic steps for the construction of a 3D reservoir model. The workflow (Fig. 1) begins with the creation of the database and its quality check. The setup of the static model then requires integrating the available geophysical and geological data into the modelling software. The stratigraphic markers selected on well trajectories are

interpreted together with the seismic horizons that correspond to the Top and Bottom reservoir surfaces and possible inconsistencies between well and seismic data are adjusted. The stratigraphic correlation provides insight into the inner reservoir structure. The geometry of the structural model combined with well log and pressure data can lead to the recognition of hydrocarbon water contacts and identification of hydraulically separated compartments, which have a sizeable impact on the dynamic simulation outcome and the production strategy of the field. Then, petrophysical characterization takes place using log and core data; at this stage, the depositional and lithological facies can be recognized and their corresponding petrophysical values (porosity, irreducible water saturation, absolute permeability) assigned. The 3D geometrical model of the reservoir is constructed by incorporating all the data from seismic interpretation, stratigraphic correlation and structural analysis. The model is later subdivided into zones and layers to honor the stratigraphic data and eventually, into the elementary units (cells) of the 3D grid. The petrophysical values are transferred into the model in the form of scaled-up well logs and then distributed in the grid by geostatistical methods using deterministic or stochastic approaches or a combination of both. In the end, the model is used for the calculation of the volume of hydrocarbons originally in place (HOIP).

Nowadays, even if the "basic steps" of the workflow remain the same, the interaction between specialists has considerably increased the quality of the resulting model, confirming the importance of "integrated reservoir studies" pointed out by various researchers (e.g. Cosentino, 2001; Benetatos and Viberti, 2010). Despite geological models being conditioned by all types of available data, the need of taking into account all uncertainties and propagating them appropriately through the modelling process still exists and represents a critical factor in order to achieve reliable results. Those uncertainties are mostly linked to the initial dataset configuration (e.g. well spacing, logged intervals), the accuracy of the measurements and the stochastic component of the geostatistical distributions adopted during modelling. Sometimes the uncertainties can be associated to more geological oriented problems, such as the extension of the geological bodies in areas not covered by seismic data or the width of a fault zone as it develops laterally from the actual fault plane. Mapping these uncertainties, evaluating their impact on both the volumetric calculations and the dynamic response of the system should be a major part of a reservoir study: the uncertainties affecting the volume of hydrocarbons originally in place can be evaluated with the reservoir static/geological model to be then propagated to the forecast phase in the case of green fields whereas the uncertainties affecting the recoverable hydrocarbon reserves can be reduced mainly through the history matching process only if there is a historical production life for the field under examination.

Modern reservoir modelling software offers the user a variety of tools to integrate all available type of data into a 3D model and it can assist in investigating and propagating the entire range of associated uncertainties through automated processes. In the cases in which particular geological conditions need to be reproduced in the model, an *ad-hoc* approach that combines the available tools might be necessary. The case presented in this paper is aimed at demonstrating how initial uncertainties can be incorporated into the modelling process and how the uncertainties can then be propagated to the dynamic modelling phase in a carbonate reservoir, so as to estimate a confidence range on the final results. To this end, we used a Discrete Fracture Network (DFN) property that is usually a part of the dataset when seismic data and fracture information are combined together. The selection of a carbonate reservoir was driven by the geological and structural complexity that is often found in this reservoir type and that can significantly affect the reliability of both the static and dynamic modelling processes. To clearly outline the main feature of the approach to fractured reservoirs and make it of general applicability, a case history is presented. This case history is representative because it comprises many of the aspects typically encountered in the study of carbonate reservoirs. The reservoir is oil bearing and subject to water drive.

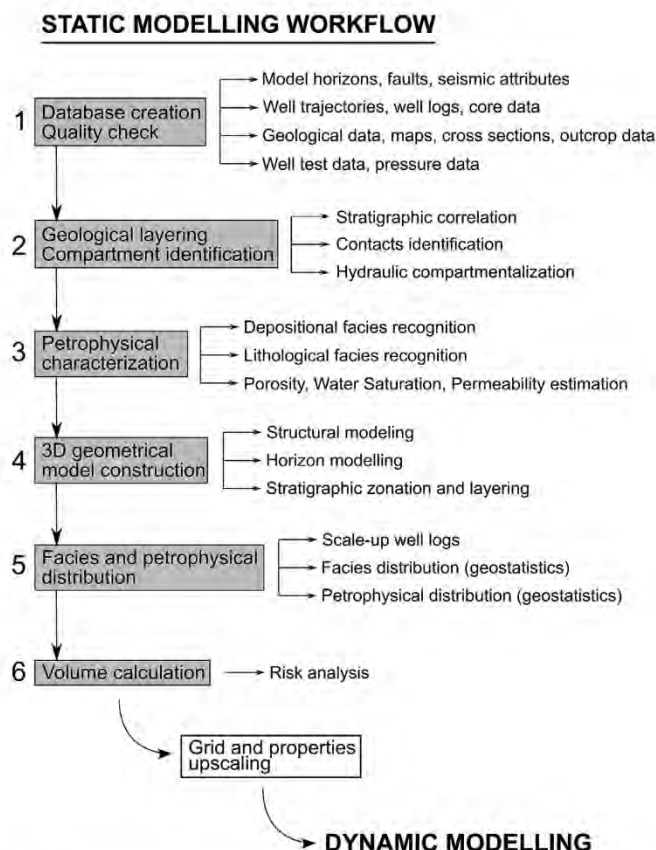


Fig. 1. Schematic representation of the workflow for reservoir static modelling.

In the following sections, the setup of the model and the investigated space of uncertainties are discussed.

### 3. Model construction

The construction of the reservoir model and the implementation of the uncertainty analysis were performed with a commercial modelling software available in the petroleum industry. The software can support all the steps of the static modelling workflow from the creation of the database to the distribution of facies or petrophysical parameters inside the 3D grid.

#### 3.1. Construction of the 3D grid

The construction of the model follows the geometrical characteristics of a retrograding carbonate platform of ramp type (e.g. [Schlaher, 2007](#); [Tucker and Wright, 2009](#)). In [Fig. 2](#) a simplified depositional facies section of the model is shown.

The Top surface of the model describes an anticlinal structure with approximate dimensions  $10 \times 5 \text{ km}^2$ . The surface depth varies from a minimum of 1050 m to a maximum of 1850 m. The Bottom surface is found at an average depth of 2000 m and it is characterized by a smoother geometry compared to the Top surface. The reservoir has a single stratigraphic zone and was vertically subdivided into 494 layers with a constant layer thickness of 2 m.

In the reservoir area a total of 18 wells were drilled, comprising 13 vertical, 3 deviated and 2 horizontal wells ([Fig. 3](#)). The bottom depth of

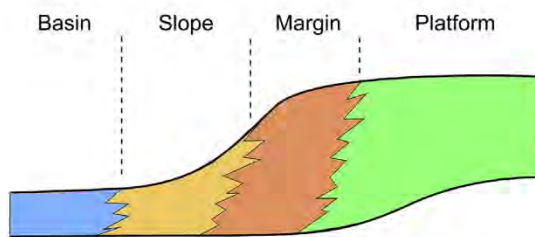


**Fig. 2.** Simplified geometry of the depositional facies corresponding to a carbonate ramp.

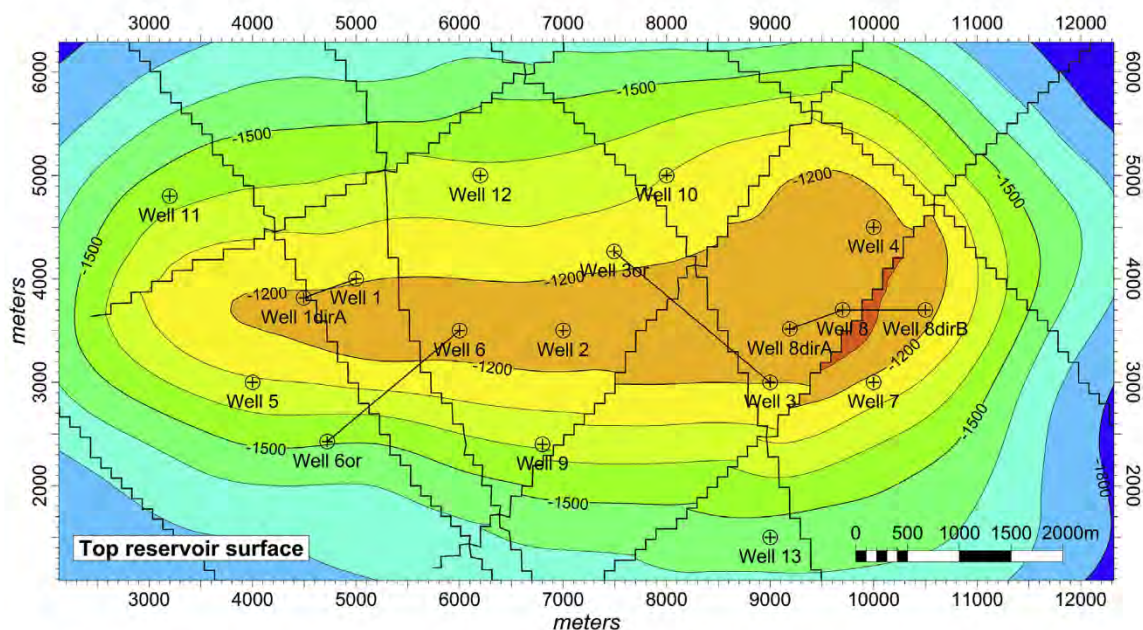


**Fig. 3.** Top reservoir map of the reservoir model. The position of the well heads in the model is shown with their corresponding name. The fault system (black lines) dislocating the Top surface is also indicated.

all vertical wells reaches the Bottom surface, while the deviated and horizontal wells are located entirely inside the reservoir zone.

The structural complexity of the reservoir is controlled by two fault systems that develop along two main directions: NW-SE and NE-SW ([Fig. 3](#)). The latter has a more significant effect on the reservoir rock creating dislocations visible on the Top reservoir surface. The direction of the faults and their distance are such as to produce significant effects on pressure propagation and fluid flow. In fact, some of the wells, especially the horizontal ones, pass through faulted zones where the number of fractures and permeability are significantly high. This is expected to induce a substantial enhancement of fluid flow and hence well production.

A fracture system was implemented to model the presence and distribution of fractures with respect to the position of the faults. A discrete fracture network (DFN) property (§ 3.4) was used as a trend for the fracture property distribution. Fractures were distributed inside the reservoir stochastically, whereas a fault-controlled fracturing system was implemented close to the fault planes.

The cells of the model have dimensions of  $100 \text{ m} \times 100 \text{ m}$  and the faults were all defined as “zig-zag” type, i.e., following the geometry of the cells, to make it easier to apply grid modifications and perform the upscaling of the petrophysical properties. The 3D grid is made up of  $105 \times 55 \times 494$  cells in the  $i \times j \times k$  direction, respectively, for a total of 2852850 cells ([Fig. 4](#)).

#### 3.2. Depositional and lithological facies

The 3D grid was subdivided internally, following the general geometry presented in [Fig. 2](#), with four basic depositional facies described briefly below ([Harris, 1985](#)):

- **Platform** depositional facies corresponding to lagoons and tidal flats sediments characterized by continuous wide sheet poorly sorted material; sediments range from carbonate sands to muds and commonly contain algal stromatolites; usually they present low porosity due to dewatering and compaction.
- **Margin** depositional facies characterized by the presence of reefs and organic buildups where there is a break in slope on the sea floor; it is often a rather narrow area of few tenths of meters wide; depending on

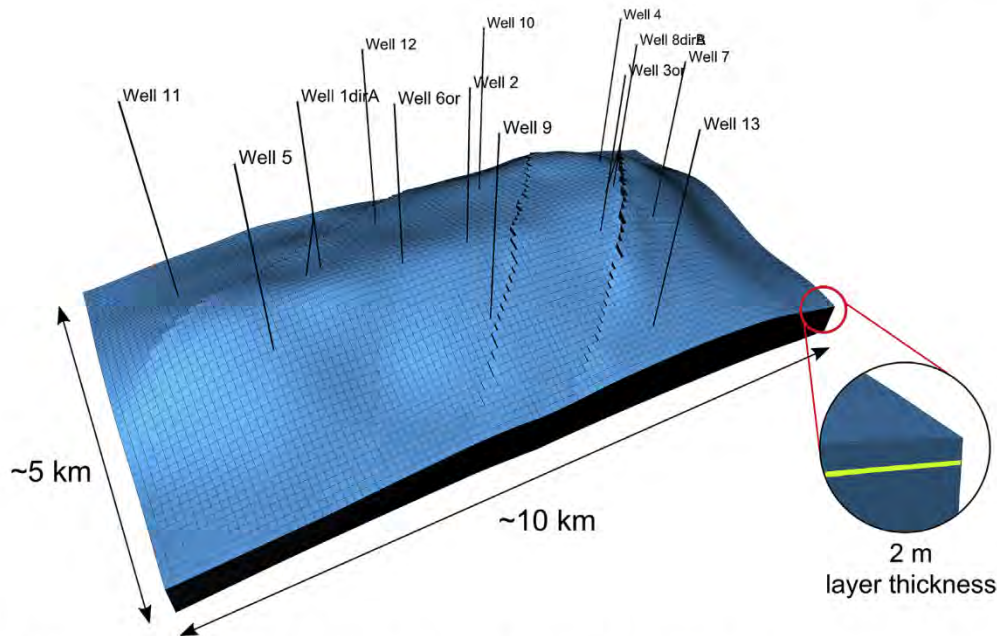


Fig. 4. Geometrical representation of the 3D grid showing the wells position, the overall dimensions and the layer thickness.

the cementing grade, there can be variations of the porosity but they are generally considered as high reservoir potential areas mostly due to rapid skeletal accumulation.

- **Slope** depositional facies including variable sediment types depending on geometrical and sedimentological characteristics; usually mud to sand size skeletal debris can be deposited in this area while coarser sediments as lower parts of turbidite sequences can also be present.
- **Basin** depositional facies characterized by pelagic sediments of very thin bedding typical of the gravitational settling that is the main mechanism of deposition in this area.

Lithological facies were distributed inside each of the depositional facies mentioned above to provide the necessary geological heterogeneity that is expected when moving from low-quality reservoir, i.e. platform facies, to high-quality reservoir, i.e. slope facies. For each depositional facies the following qualitative lithological facies were assigned (Sarg et al., 1999):

- Platform: Mudstone
- Margin: Grainstone (shoal)
- Slope: Packstone, Grainstone (bioclastic)
- Basin: Limestone (fine)

An additional lithological facies linked to hydrothermal dolomitization was added to accurately describe the reservoir geology even if this meant increasing the complexity of the model. According to Langhorne and Graham (2006) and references therein, hydrothermal dolomitization can be defined as the deposition of minerals occurring under burial conditions with elevated temperature (higher than the one of surrounding rocks) and pore pressure. Commonly the deposition occurs peripherally or along fault or fracture systems (Fig. 5). In our model we considered that the faults that could eventually become pathways for hydrothermal fluids were controlled by an attribute probability map produced during the geophysical interpretation. This map was used as a trend during the distribution of the dolomitic facies (§ 4).

### 3.3. Fractures and discrete fracture network (DFN)

In fractured reservoir studies it is common to use attribute properties that are the outcome of seismic interpretation (Guerreiro et al., 2000;

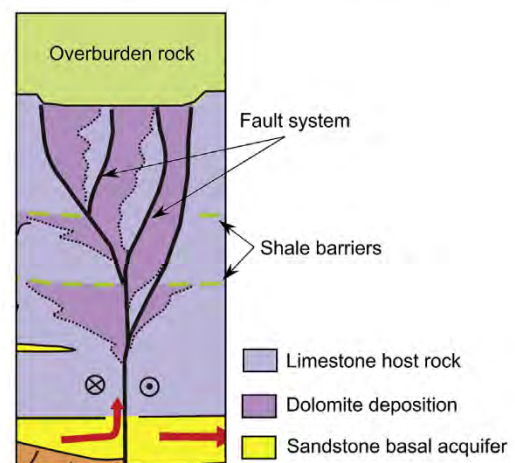


Fig. 5. Schematic representation of dolomitization occurring through a hydrothermal fluid-flow system originating at a sandstone basal aquifer and propagating upward through a fault network and the presence of shaly barriers (Figure modified from Davis and Smith, 2006).

Bloch et al., 2003). Sometimes, to identify areas that exhibit more intense fracturing, special attribute maps are created (e.g. Bahorich and Farmer, 1995; Marfurt et al., 1998, 1999; Gersztenkorn and Marfurt, 1999) that assist geologists to better characterize the fracture system and to optimize drilling directions for new wells. For the creation of a fracture network model it is usually necessary to combine regional geological information, structural data, well data and seismic data. Furthermore, depending on the structural evolution of the area, fault movements can be responsible for additional fracturing events in the vicinity of the fault planes creating damage zones (Choi et al., 2016 and references therein) that can extend from few meters to hundreds of meters and that can have an important impact on fluid flow (Fig. 6).

In this work, we used a DFN property driven by the fault system geometry and representing the fracture intensity, decreasing with the distance from the fault planes. The values of the constructed property represent fracture probability and thus vary from 0 to 100%. The same property was also used to calculate fracture porosity using a Gaussian random function simulation with a mean value of 0.5% (Fig. 7).

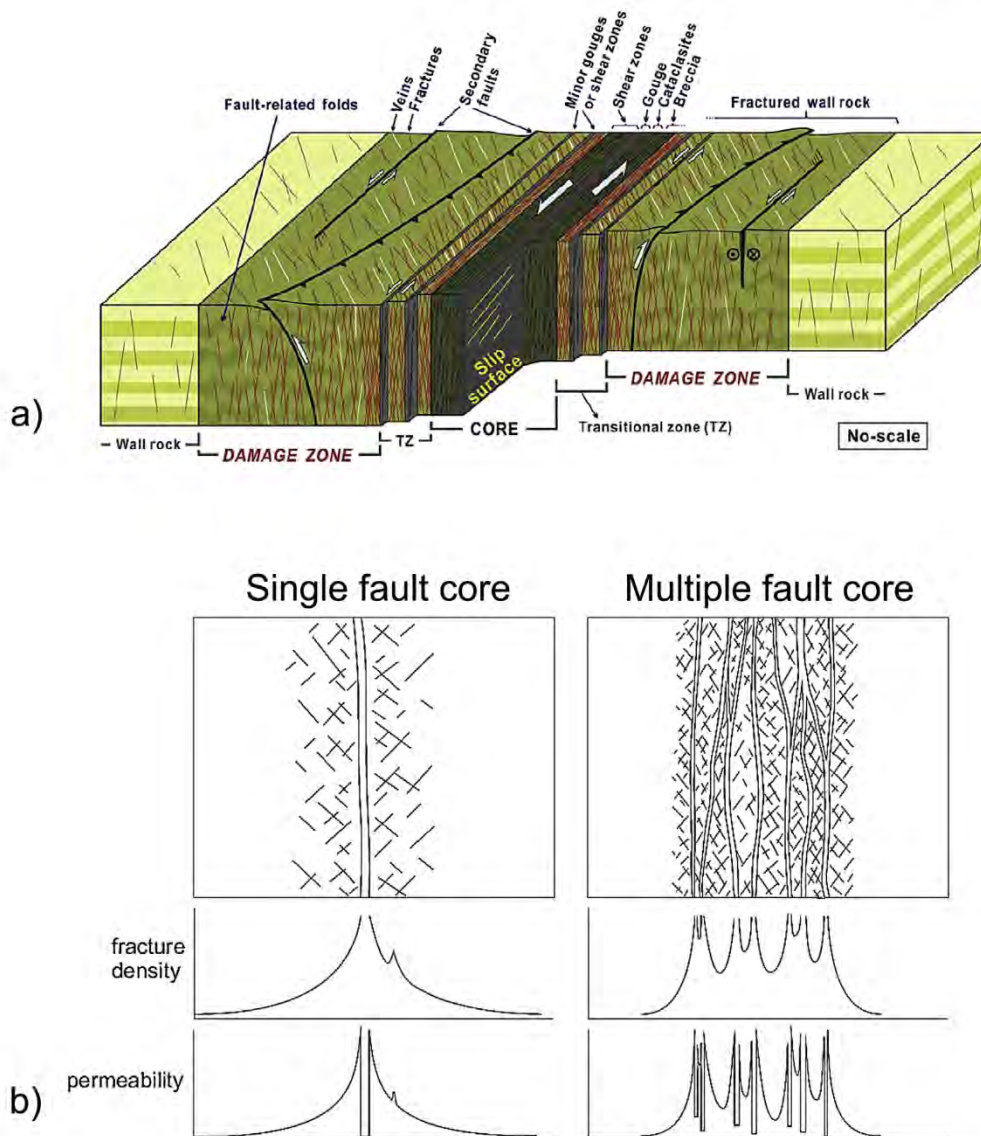


Fig. 6. (a) Schematic representation of the variation of the deformation inside a fault zone accompanied by the development of various fault-rock types and secondary structures (fractures, folds, faults) in different parts of the fault zone (Figure from Choi et al., 2016). (b) Fracture density and permeability in relation to the fault structure complexity for single fault core (left) and multiple fault core (right) (Figure from Faulkner et al., 2010).

### 3.4. Petrophysical parameters

In fractured carbonate reservoirs two distinct, interacting porous systems are typically present: a primary porous system, the matrix, usually containing most of the hydrocarbons (thus having storage capacity), and a secondary porous system, the fracture network, typically providing connectivity in the reservoir and between the wells.

Therefore, when modelling the petrophysical parameters of carbonate reservoirs, both the matrix and the fracture systems must be characterized. From a dynamic point of view, depending on the interaction between the matrix and the fractures and, specifically, on the process by which the matrix recharges the fractures during production, one of the following three modelling approaches can be adopted:

- Single porosity approach: a single equivalent medium comprising both the matrix and the fractures is modelled and characterized in terms of equivalent petrophysical properties.
- Double porosity approach (Teutsch, 1993): the matrix and fracture systems are defined separately and their coupling is modelled through a specific parameter (sigma factor) describing their interaction. The

weak point of this approach is the uncertainty related to the value assigned to the sigma factor.

- Double porosity - Double permeability approach: the matrix and fracture systems are defined as two separate porous and permeable porous media, and two sets of fluid flow equations need to be solved (e.g. Bai et al., 1993; Vogel et al., 2000). This approach is computationally very demanding, and actually recommended only in a few cases, such as in the presence of negligible viscous forces due to low fluid velocities (i.e. gravitational and capillary forces govern production)

In our work, the assignment of petrophysical parameters to the reservoir model was performed separately for the rock matrix and for the fracture system. Then, a "final", equivalent property (associated with the single porosity approach) was constructed for each petrophysical property (porosity, irreducible water saturation and absolute permeability) taking into account both the matrix and the fracture system contributions. The adoption of an equivalent, single porosity approach, if properly validated through comparison with standard double porosity and double porosity - double permeability models, is a common practice in the

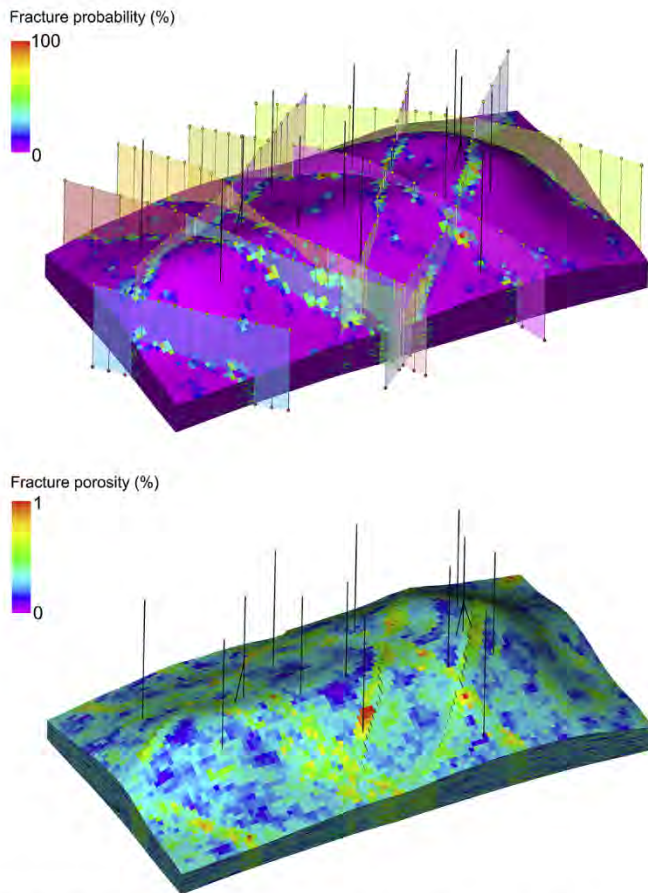


Fig. 7. 3D view of the discrete fracture network (DFN) property (Top) showing fracture probability and the corresponding distribution of the fracture porosity values (Bottom).

petroleum industry for modelling purposes. The approach provides reliable results with a significant reduction of the computational time and the possibility to performing a larger number simulations and thus obtaining better reservoir management (Quintana Saalfeld et al., 2016 and references therein).

#### 3.4.1. Matrix petrophysical parameters

Each lithological facies was assigned a representative porosity distribution, taken from the literature, expressed by a mean value and a standard deviation to differentiate between best and worse quality reservoir rocks.

Irreducible water saturation was calculated using a formula proposed by Buckles (1965) and modified by Holmes et al. (2009) suggesting that the product of porosity and irreducible water saturation in a formation remains constant and can be expressed as:

$$\Phi^Q \times S_{wi} = C$$

where Q and C are constants.

In the case presented in this work the constant C is considered as an uncertain parameter, whereas  $Q = 1.1$  (Holmes et al., 2009).

Absolute permeability values were assigned to the reservoir matrix using the following k- $\Phi$  relation, based on laboratory sample measurements:

$$\text{Permeability} = 1.5 \times e^{\text{Porosity} \times 50}$$

#### 3.4.2. Fracture petrophysical parameters

The fracture porosity was distributed using the DFN property as a

trend. It was assigned a mean porosity value of  $\Phi_{\text{fracture}} = 0.5\% (\pm 0.2\%)$ .

Fracture irreducible water saturation was assumed negligible and therefore given the value of  $S_{wi} = 0$ .

Fracture absolute permeability values were distributed in the 3D grid using the DFN property as a trend. Since permeability for the fracture network was considered as an unknown parameter, two distinct k- $\Phi$  relations with mean permeability values of 1 and 10 Darcy, respectively, were implemented.

#### 3.4.3. Equivalent petrophysical parameters (single porosity approach)

The equivalent petrophysical parameters used in the dynamic model were derived from both the petrophysical parameters of the matrix and those of the fractures and hereafter are referred to as “equivalent” properties.

The equivalent porosity is the total porosity, i.e., the simple sum of matrix and fracture porosities, as follows:

$$\Phi_{\text{total}} = \Phi_{\text{matrix}} + \Phi_{\text{fractures}}$$

the equivalent irreducible water saturation was calculated based on a porosity-weighted average of the matrix and fracture irreducible water saturation values, as follows (considering  $S_{wi \text{ fracture}} = 0$ ):

$$S_{w \text{ total}} = \frac{S_{wi \text{ matrix}} \times \Phi_{\text{matrix}}}{\Phi_{\text{matrix}} + \Phi_{\text{fracture}}}$$

The equivalent absolute permeability was obtained by distributing the values of matrix permeability and then by overwriting the initially assigned values with the fracture permeability values in every cell where the fracture intensity and/or the distance from the fault planes (as defined by the DFN model) was higher than a given threshold value. By varying the threshold value, different connectivity scenarios could be tested: the lower the threshold value, the more dominant is the fracture network at the expenses of the matrix background.

Once the petrophysical properties (equivalent porosity, equivalent irreducible water saturation and equivalent absolute permeability) were defined, they were properly upscaled according to the layering adopted in subsequent the dynamic modelling phase and then used to populate the dynamic model.

## 4. Model uncertainties

Different types of uncertainties were considered in the model to cover a variety of situations that can be encountered during a fractured carbonate reservoir study. Some are linked to the geological complexity due to sediment deposition and expressed through the depositional facies geometry and presence of different lithological facies, while others are linked to the variations of petrophysical values.

### 4.1. Dip angle and azimuth of facies

The first uncertainty of the model is related to the dip angle and azimuth of the depositional facies. In several cases where the well coverage is low or where there is little control over the flanks of an anticline structure, it can be useful to evaluate the effect of changes of the dip and azimuth of the facies on the calculation of the volume of hydrocarbons.

In the static model the distribution of depositional facies was performed using the facies modelling process. During this step of the workflow, the user can define an upper and a lower boundary for the facies and the azimuth along which the distribution will occur. During the uncertainty analyses there is the need to change the angle of the facies boundaries in order to try different deposition orientations but this results in recalculating all facies borders, thus losing their predefined geometry. Since the facies borders should preserve the general geometry designed by the user, the azimuth variation in the uncertainty analysis workflow can become a challenging task. Accordingly, a set of properties of different depositional facies geometries was created to cover the

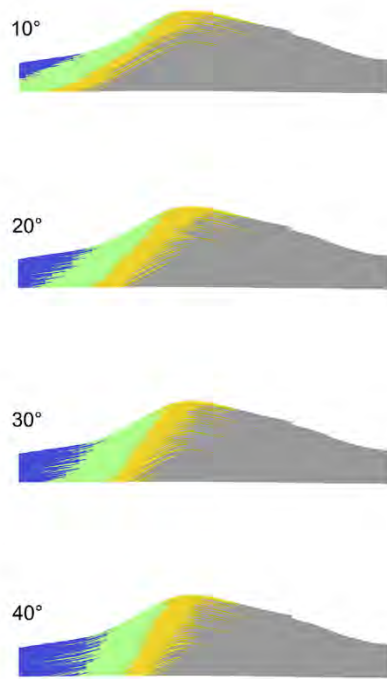


**Fig. 8.** Examples of the variation of the dip angle of the depositional facies ranging from 10° to 40°.

desired range of possible dip angles and azimuths. These properties were stored in a folder from which, during the uncertainty analysis, the software could pick randomly using the selected set as a trend during the depositional facies distribution. Four different dip angles were selected ranging from 10° to 40° (Fig. 8) and for each of them 20 realizations were performed allowing the azimuth to vary randomly between -10° to 10°; in total, 80 sets of properties with different dip values and azimuth were produced. During the modelling process, different seed numbers were controlling the stochastic component of each realization.

#### 4.2. Dolomitization areas

“Hydrothermal dolomitization” is a particular geological process that can affect fractured dolomite or carbonate formations (Warren, 2000;

Davis and Smith, 2006; Labourdette et al., 2007; Barale et al., 2013; Morrow, 2016). The fluids usually invade the reservoir zone through the fracture system and affect the nearby lithologies (Fig. 5). To recreate the characteristic “flower” shape of the altered zone, a simple mathematical formula was used to ensure a wide affected area close to the Top horizon that progressively becomes thinner as moving deeper. For this calculation it was necessary to use a combination of grid properties. The first property represents the distance of each cell from every fault of the grid (Fault\_dist). The second one contains the normalized values of the distance of each cell from the reservoir Top (Top\_dist), ranging from 1 at the top and progressively decreasing with depth. Using the following mathematical formula it is possible to obtain the desired geometrical shape of the dolomitization areas in relation to the fault planes:

$$\text{Dolomitization\_geometry} = \text{Fault\_dist} \times \text{Top\_dist}^5$$

The lateral extension of the dolomitization zones was controlled by a map derived from seismic interpretation (Fig. 9). The seismic attribute shown in the map gives the probability of occurrence of dolomitic facies. Three discrete properties of probability ranges (high, medium and low), corresponding to a pessimistic, a neutral and an optimistic extension of the dolomitic facies, were created (Fig. 10). During the uncertainty analysis the different properties of the dolomitization probability were combined randomly with those of the dolomitization geometrical shape so as to generate the necessary property for the facies distribution.

#### 4.3. Matrix porosity

Matrix porosity values of all the lithological facies were included in the uncertainty analysis. For each facies the porosity was allowed to vary  $\pm 20\%$  of the mean values provided below:

- Mudstone:  $\Phi_{\text{mean}} = 2\%$
- Grainstone (shoal):  $\Phi_{\text{mean}} = 3\%$
- Packstone:  $\Phi_{\text{mean}} = 4\%$
- Grainstone (bioclastic):  $\Phi_{\text{mean}} = 5\%$
- Limestone (fine):  $\Phi_{\text{mean}} = 2\%$
- Dolomite:  $\Phi_{\text{mean}} = 9\%$

#### 4.4. Matrix irreducible water saturation

The matrix irreducible water saturation for each lithology was

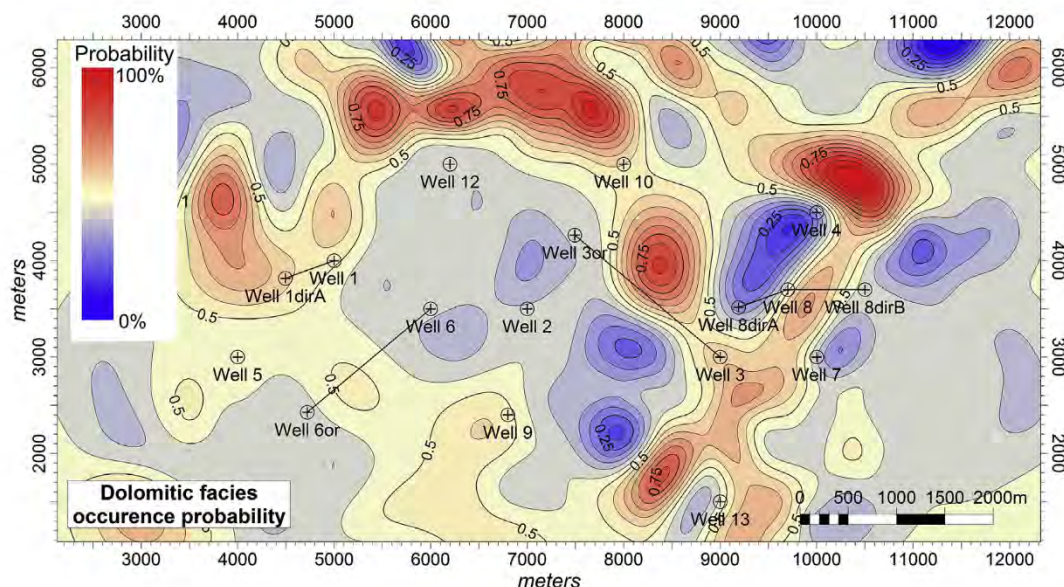


**Fig. 9.** Attribute map showing the probability of occurrence of dolomitic facies on the upper part of the reservoir.

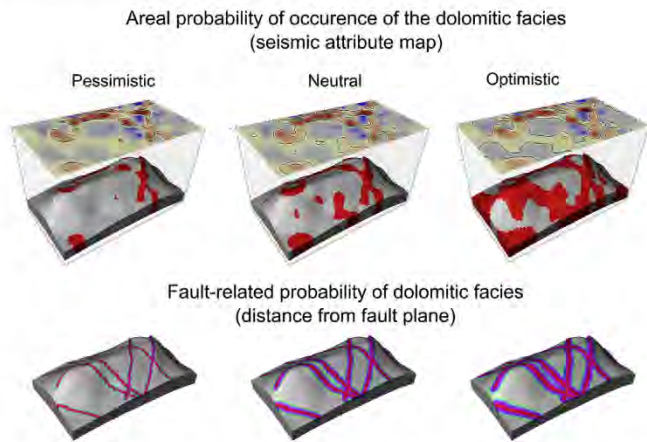


**Fig. 10.** (Top) Areal probability of occurrence of the dolomitic facies as inferred from the seismic attribute map. (Bottom) Fault-related probability of occurrence of the dolomitic facies for three distances from the fault plane.

calculated based on the formula and base values proposed by Buckles (1965) and modified by Holmes et al. (2009). A constant of 0.01 was chosen as the base value with a 0.008–0.012 variation, while the value of  $Q$  was set equal to 1.1. In Fig. 11 the three  $S_{wi}$ - $\Phi$  curves used in the uncertainty analysis are shown.

#### 4.5. Absolute permeability

Absolute permeability values were distributed separately for the matrix and for the fracture systems. In the case of the matrix (background system), a  $k$ - $\Phi$  correlation was used (Fig. 12) providing an average permeability of almost 10 mD.

Permeability values for the fracture system were also calculated using a pair of  $k$ - $\Phi$  relations. The mathematical relations were chosen to produce average permeability values of 1 and 10 Darcy, respectively. During the distribution of fracture permeability values in the model the fracture intensity, and/or distance from the fault planes (i.e., fracture probability, as defined by the employed DFN model) was used as a trend. An example

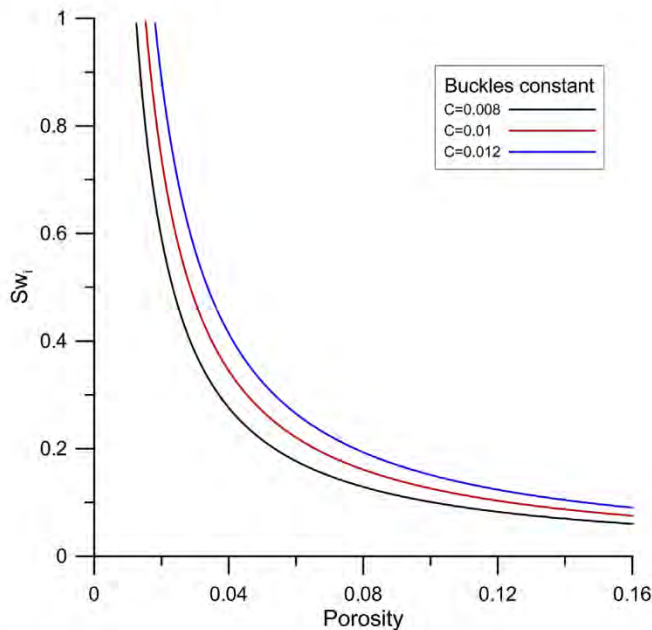


**Fig. 11.** Relation between porosity and irreducible water saturation as proposed by Buckles (1965) and modified by Holmes et al. (2009) for 3 different constants.

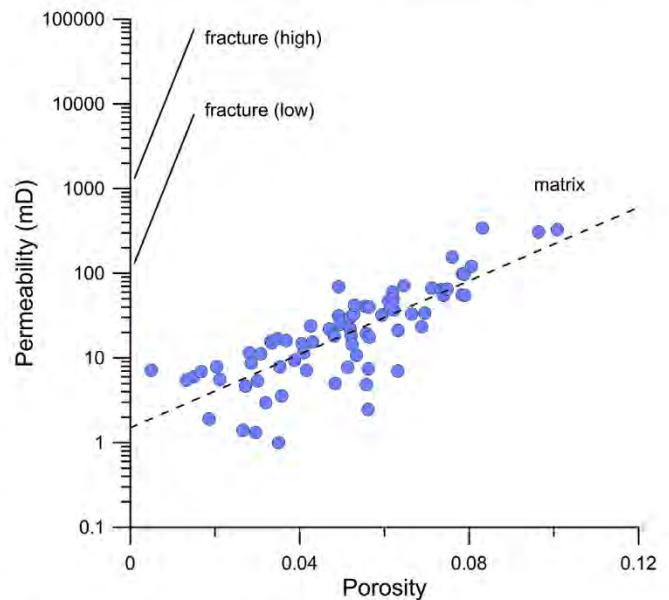


**Fig. 12.** Porosity – permeability relation ( $k$ - $\Phi$ ) for the reservoir matrix (blue circles) and for the fractures (linear functions). In the case of the fracture permeability two linear regression curves corresponding to a low case (average permeability of 1 D) and a high case (average permeability of 10 D) were used.

of permeability distribution for the fracture system is shown in Fig. 13.

For the definition of the equivalent absolute permeability (matrix + fractures) distributions, the following parameters were considered as uncertain:

- matrix/fracture threshold value, defined on the basis of the fracture intensity/probability values associated with the DFN model; this parameter was used for discriminating the most intensely fractured areas (in which the equivalent permeability was associated with the fracture system) from areas with scarce or non-existent fracture intensity (in which the equivalent permeability was associated with the matrix system only);
- constant “ $n$ ” of the  $k$ - $\Phi$  relation ( $k = 10[125 * \Phi + n]$ ) associated with the fracture system; this parameter defines the entity of the absolute permeability values assigned to the areas of the reservoir in which the fracture intensity/probability is higher than the considered threshold value.

For the definition of the matrix/fracture threshold values a 0.02–0.08 range with uniform probability was considered, whereas the value of the constant “ $n$ ” of the  $k$ - $\Phi$  correlation associated to the fracture system was assumed to vary according to a continuous triangular distribution, with a minimum of 2, a maximum of 3 and with a central value of 2.5. Fig. 14 shows an example of how the equivalent permeability was constructed.

## 5. Automated workflow

All the above-mentioned uncertainties were introduced into an automated workflow to evaluate the effect on the calculation of the volume of hydrocarbon originally in place as well as to evaluate the performance of the model during dynamic simulations.

A workflow was implemented, and automatically run, to vary the input data accounting for the variability of all the selected uncertainties, export results and perform calculations.

The workflow had the necessary steps to reproduce a 3D static model from the structural modelling to the volumetric calculation. In this case the construction of the carbonate reservoir model and the execution of the uncertainty analysis followed the standard steps of the static modelling process. It began with the structural modelling, which

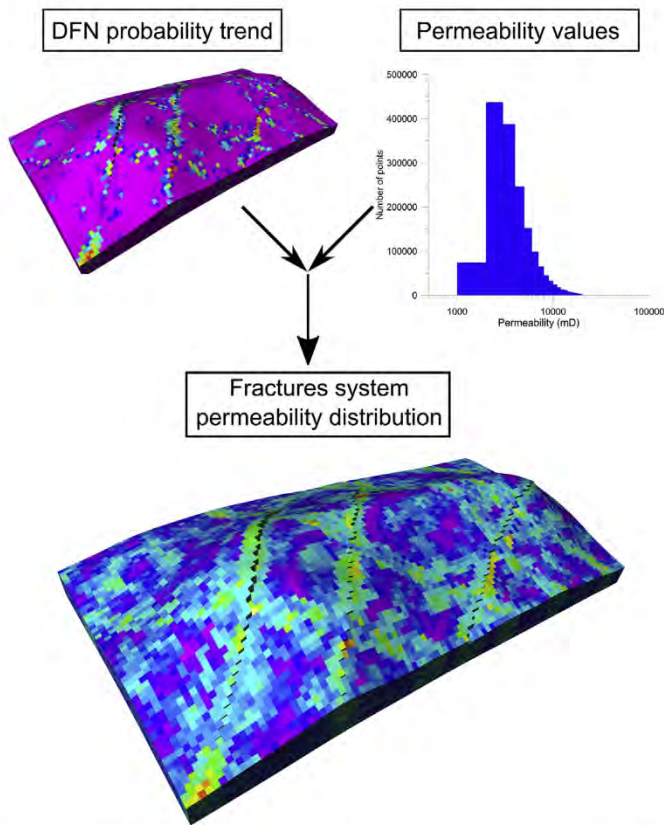


Fig. 13. Workflow for the generation of the fracture permeability values. The DFN property was used as a trend to guide the distribution of the permeability values defined by a  $k-\Phi$  relation.

provides the skeleton of the grid, and continued with the Horizon modelling, where the Top and Bottom horizons of the reservoir are inserted into the model. Then the 3D grid was constructed using specific cell dimensions and the fault system was incorporated into the grid. At this point the basic layering was performed for the logs of porosity and facies to be scaled-up, ending the preliminary part of the model construction and resulting in a fully functional 3D grid including scaled-up petrophysical and lithological properties. The rest of the workflow was dedicated to the construction of the properties used in the uncertainty analysis and to the definition of the selection criteria for the different runs. In Fig. 15 a schematic workflow is presented with indication of the specific actions taken at each step. The uncertainty analysis included different types of parameters that were either predefined grid properties or numerical value ranges; in both cases the entire uncertainty space was sampled. The uncertainty analysis was performed by using either uniform distributions (all the values share equal probabilities of occurrence) or triangular/normal distributions (higher probability of occurrence to the values closer to the mean values) for each of the uncertain parameters.

After the definition of the uncertain parameters, the parameters used to define the depositional facies geometry (dip and azimuth) and the extent and geometry of the dolomitic facies were selected stochastically. The first property distributed in the grid was the lithological facies. The variogram for lithological facies distribution was set to vary both horizontally and vertically while the seed number changed at each run. The seed number is used very often in geostatistical distributions because it preserves the random nature of the sequence according to which values are assigned in each cell of the model. Similarly, the matrix petrophysical properties were distributed inside each lithological facies with normal distributions defined by a variable mean value and standard deviation. Then the fracture porosity was calculated and added to the matrix

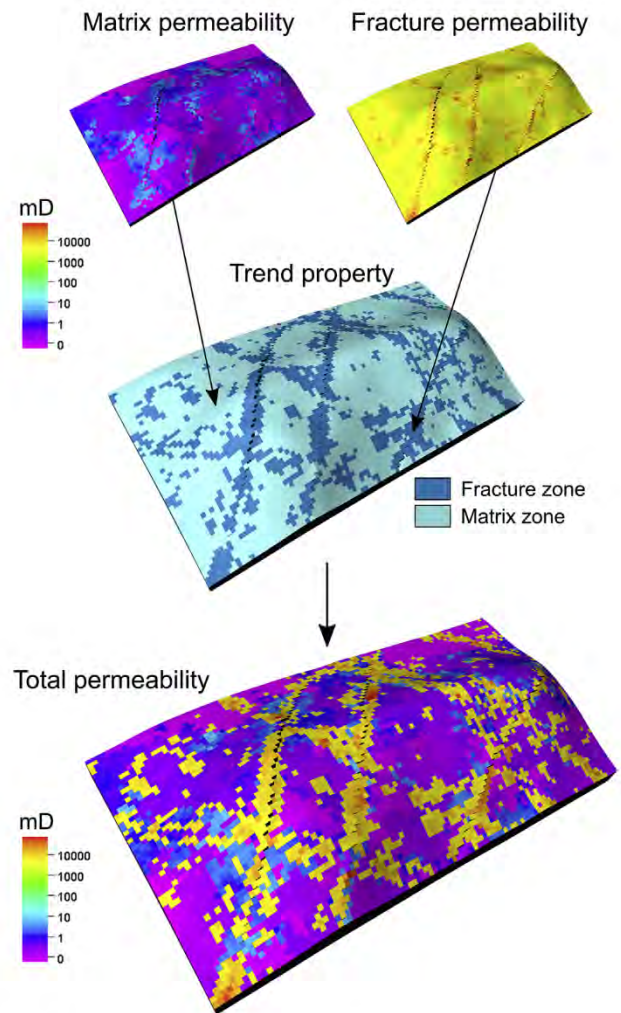


Fig. 14. Calculation of the equivalent absolute permeability property by combining the matrix and the fracture permeability. The intermediate “trend property” serves as a guide during the execution of the workflow to identify the cells with significant fracture intensity/probability.

porosity values to obtain the equivalent total porosity. The matrix irreducible water saturation calculation was performed using the Buckley formula that was previously selected. The equivalent irreducible water saturation was then calculated. The equivalent absolute permeability property was constructed by combining the matrix and the fracture permeability properties in the way described in the previous sections. Each run was concluded with the volumetric calculation for that particular selection of properties and petrophysical values. In all the uncertainty values used to perform the runs with the static model are summarized.

The volumetric results can be visualized as a histogram providing the  $P_{10}$ ,  $P_{50}$  and  $P_{90}$  percentiles of the volume of the oil originally in place (OOIP). These percentiles express the variation of the volume of hydrocarbons originally in place associated with the considered uncertainty parameters and values. In Fig. 16 the results of 1000 runs are presented. The configuration of the model and the selected uncertainties resulted in a  $P_{50} = 228 \times 10^6 \text{ m}^3_{\text{SC}}$  of oil originally in place (OOIP).

## 6. Dynamic modelling

The dynamic model used in this study is a Corner Point model, Black Oil, built with a 3D numerical simulator.

Preliminary dedicated sensitivities were performed on selected geological realizations to compare the simulated response of a standard

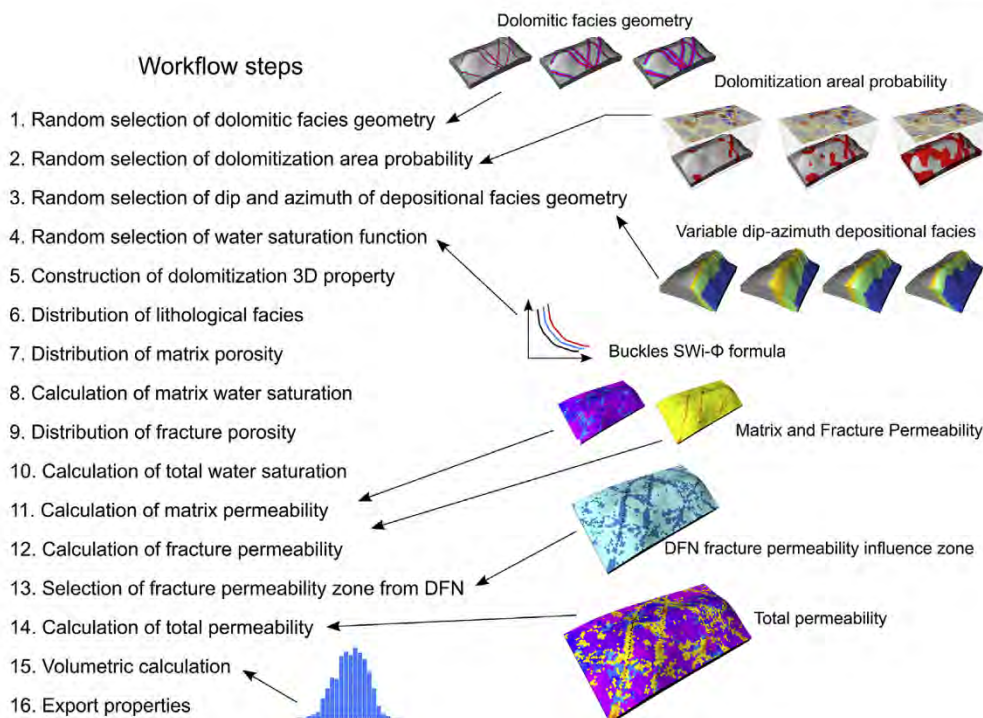


Fig. 15. Schematic uncertainty analysis workflow with a brief description of each step. Details on the actions taken at each step are described in the text.

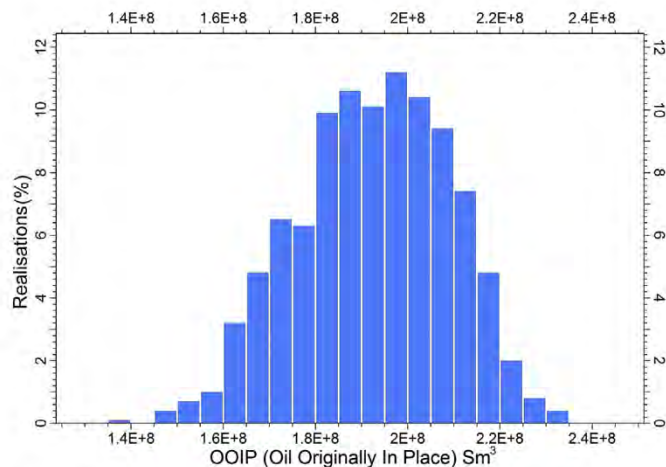


Fig. 16. Histogram of the OOIP (Oil Originally In Place) values based on 1000 runs of the uncertainty analysis workflow.

double porosity approach to that of an equivalent single porosity model. Results proved that the latter approach could properly and reliably describe the dynamic behavior of the system under examination. Therefore, a single porosity approach was implemented in the dynamic model assuming that the dynamic behavior of the system was dictated by a single equivalent porous medium comprising both matrix and fractures. This choice allowed the reduction of computational times and the possibility of increasing the number of realizations to be tested during the risk analysis (Quintana Saalfeld et al., 2016 and references therein).

6.1. Set up of the dynamic model

The high number of cells of the original static model (105 × 55 × 494 cells in the i × j × k direction, respectively, for a total of 2852850 cells) made the coarsening of the grid mandatory to reduce the computational time of the dynamic simulations. To this end, the original layering

defined in the static model (with a thickness of each layer equal to 2 m) was modified into a uniform layering of 12 m. Also, cells located below the original oil water contact were deactivated and an infinite, analytical bottom aquifer, implemented according to the Carter Tracy approach (Carter and Tracy, 1960), was adopted in the dynamic model to reproduce the strong water drive recognized from the production history of the field. After the up-gridding process, the dynamic model comprised 105 × 55 × 166 cells in the i × j × k direction, respectively, for a total of 958650 cells, of which 66480 active.

Fig. 17 shows a 3D view of the dynamic model with the distribution of depth values in the active cells.

6.1.1. Petrophysical parameters

The dynamic model was populated with the petrophysical properties (equivalent porosity, equivalent irreducible water saturation and equivalent absolute permeability) defined in the static modelling phase (section 3.4.3) and up-scaled according to the 12-m layering. The overall

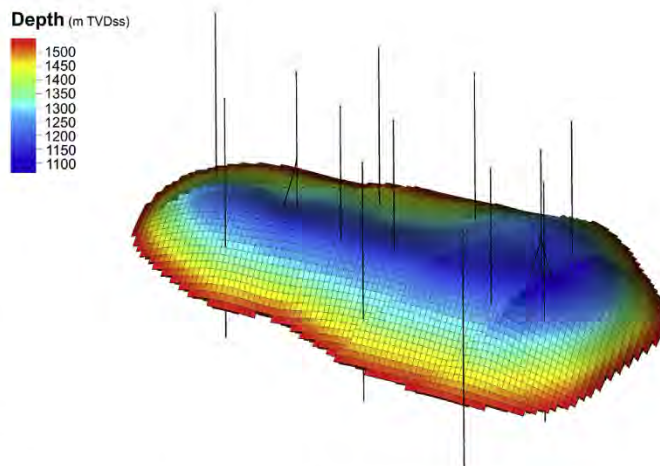


Fig. 17. 3D view of the dynamic model grid.

reservoir permeability was assumed to be isotropic. The distribution of the petrophysical properties in the dynamic model for a reference, intermediate geological realization is shown in Fig. 18.

### 6.1.2. PVT data

The reservoir is oil-bearing. The oil is a dead, heavy oil (15 °API). Oil formation volume factor ( $B_o$ ) and oil viscosity at initial reservoir pressure are equal to  $1.06 \text{ m}^3/\text{m}_{\text{SC}}^3$  and 5 cP, respectively.

The formation water has a salinity of 30 g/L NaCl; based on the correlations available in the literature, a relative density of 1.02 (w.r.t. pure water) was defined.

Water viscosity was calculated with the Osif correlation (Craft and Hawkins, 1991) and was set equal to 0.7 cP, while water compressibility was calculated with the McCain correlation (Craft and Hawkins, 1991) and set equal to  $3.8 \times 10^{-5} \text{ bar}^{-1}$ .

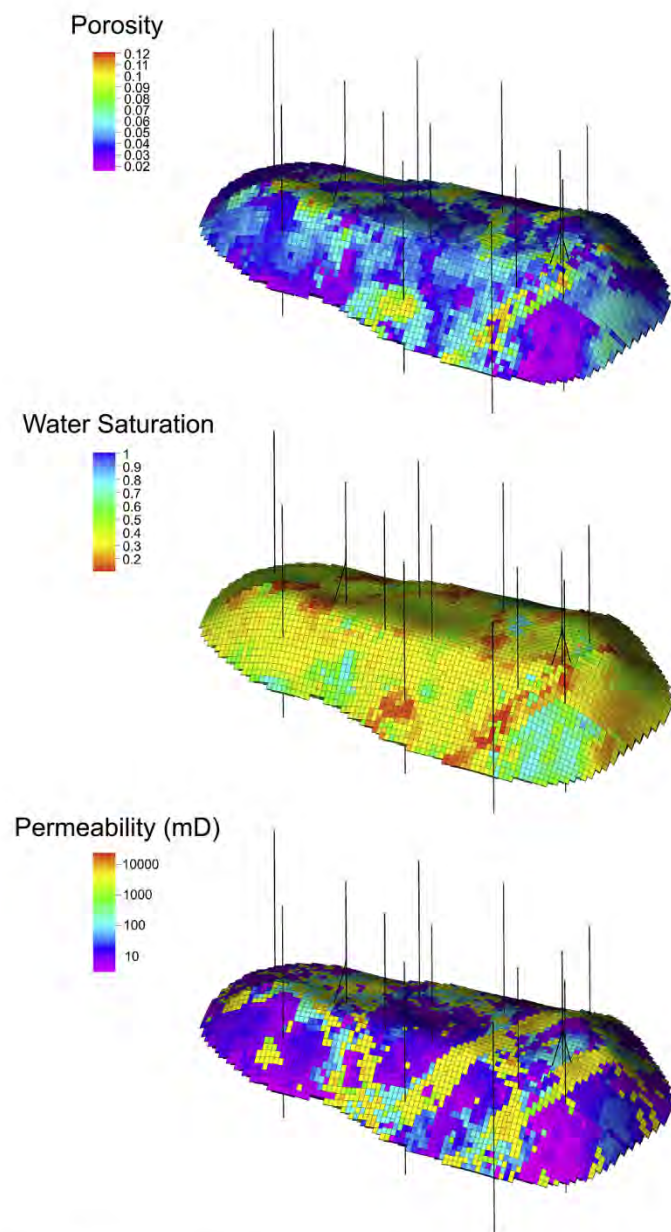


Fig. 18. Distribution of the petrophysical properties (equivalent porosity, equivalent irreducible water saturation, equivalent absolute permeability) in the dynamic model.

### 6.1.3. Rock and rock-fluid interaction parameters

Four matrix samples had been retrieved and laboratory data and special core analysis (SCAL) were available for the reservoir under analysis. Oil-water relative permeability curves were generated through the well-known Corey formulation (Baker, 1998), matching the experiments with a Corey exponent of 4 for both oil ( $N_o$ ) and water ( $N_w$ ) (Fig. 19a).

Relative permeability curves were then normalized (defined in a general 0–1 range), and compared with standard relative permeability curves for a fractured system (Corey exponent equal to 1 for both oil and water). A set of pseudo relative permeability curves for the single equivalent porous system (matrix + fractures) was defined with  $N_o = 2$  and  $N_w = 2$  and implemented in the dynamic model (Fig. 19b).

Normalized pseudo relative curves were then scaled based on the following end points (end point scaling):

$S_{wi}$ : distribution related to a given static modelling realization (equivalent irreducible water saturation distribution).

$S_{or}$ : 10% (residual oil saturation).

$k_{r,w}$ : 0.50 (water relative permeability at residual conditions,  $S_w = 1 - S_{or}$ ).

Capillary pressures were implemented in the dynamic model with maximum capillary pressure values @  $S_{wi}$  equal to 0.9 bar. The rock compressibility value was set equal to  $3.5 \times 10^{-5} \text{ bar}^{-1}$  for dynamic simulations.

## 6.2. Initialization

The initial pressure ( $p_i$ ) was set equal to 135 bar<sub>a</sub> at the reference depth (datum) of 1300 m TVD ss. The initial oil-water contact (OWCi) was defined at 1500 m TVD ss. A single equilibration region was implemented in the dynamic model.

The model was initialized by defining the initial distribution of pressure and fluid saturation values for a reference geological realization. A check of the initial hydrostatic equilibrium was performed and the original oil in place (OOIP) was calculated and compared with the corresponding static estimate. The initial oil saturation and the initial pressure distributions resulting from the initialization phase are shown in Fig. 20.

## 6.3. Forecast

After the initialization phase, the dynamic model was used to simulate the future behavior of the field, taking into account the uncertainties associated with the petrophysical characterization as defined in the static modelling phase (section 4) through a dedicated risk analysis meant to evaluate the propagation of such uncertainties and their impact on the results of the numerical simulations.

### 6.3.1. Methodology

The forecast phase for the evaluation of the field development was implemented according to the following workflow:

- definition of the reference development plan;
- definition of uncertain parameters;
- execution of risk analysis and statistical analysis of results.

### 6.3.2. Development scheme, production targets and constraints

A production time frame of 12 years was considered for the forecast phase. Four wells were set as active for the development of the field: 1 dir A, 3 or, 6 or and 8 dir B (Fig. 21).

Based on the available field data, active wells were controlled by a target, initial liquid rate equal to 3000  $\text{m}_{\text{SC}}^3/\text{day}$  and constrained by a minimum bottom hole flowing pressure of 30 bar. All producers were equipped with ESPs (artificial lift). A maximum watercut of 90% and a minimum economical oil rate equal to 20  $\text{m}_{\text{SC}}^3/\text{day}$  were assigned to each well. At field scale, a maximum production liquid rate constraint equal to

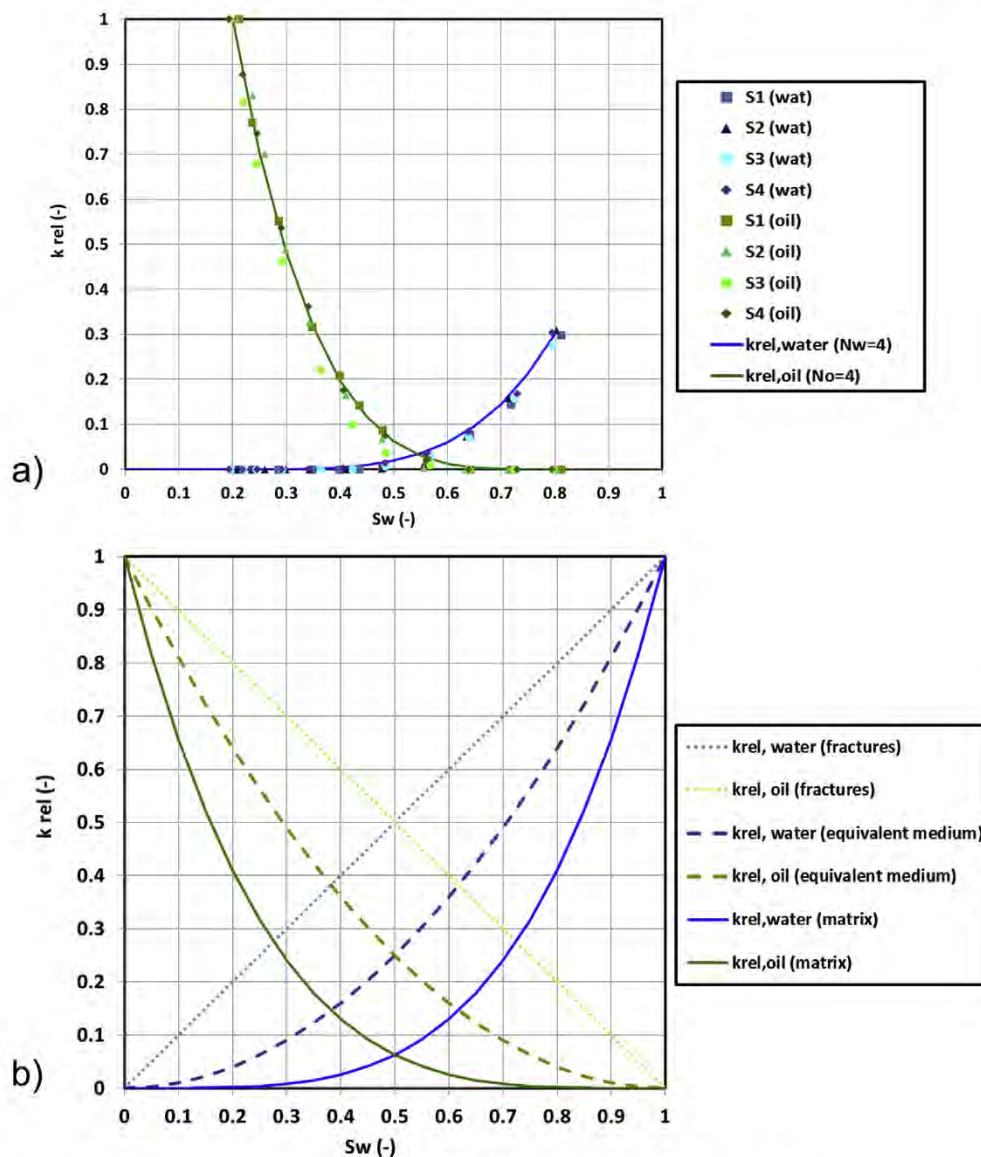


Fig. 19. (a) Oil-water relative permeability curves for the matrix system; (b) normalized relative permeability curves for the single equivalent porous system (matrix + fractures).

10000  $m^3_{SC}/day$  was also assigned.

### 6.3.3. Definition of uncertain parameters

The risk analysis for the dynamic model was defined on the basis of the results deriving from the risk analysis previously performed for the static model, using the same workflow for the definition of the equivalent petrophysical properties (porosity, irreducible water saturation and absolute permeability).

Starting from the 1000 realizations defined in the static modelling phase, a Monte Carlo sampling was adopted to define a total of 300 realizations, each characterized by a total porosity map, by an equivalent irreducible water saturation map and by an equivalent absolute permeability map. The 300 realizations were selectively sampled so as to define a statistically representative distribution of the OOIP values also for the dynamic simulations.

The number of realizations (300) was high enough to be statistically representative. The representativeness of the realizations was verified after performing the dynamic simulations, by examining the stabilization of the statistical parameters (mean and percentiles) associated with the output as a function of the increasing number of samples.

### 6.3.4. Results of the forecast phase

The results of the 300 simulations in terms of cumulative oil production and oil recovery factor (RF) @12 years are shown as histograms in Fig. 22. The following percentiles were evaluated at the end of the risk analysis:

- P10: Cumulative oil production =  $24.2 \times 10^6 m^3_{SC}$ ; RF = 13.6%
- P50: Cumulative oil production =  $26.6 \times 10^6 m^3_{SC}$ ; RF = 15.2%
- P90: Cumulative oil production =  $29.5 \times 10^6 m^3_{SC}$ ; RF = 17.0%

Fig. 23a and b displays the plots with the evolution in time of the field oil production rate and of the cumulative oil production, respectively, for the 300 simulated runs.

## 7. Conclusions

In this paper we presented a reservoir modelling workflow for handling uncertainties in a carbonate reservoir. Workflows are useful tools in reservoir engineering because they can help to systematically explore the uncertainty space and provide an estimation of the impact of

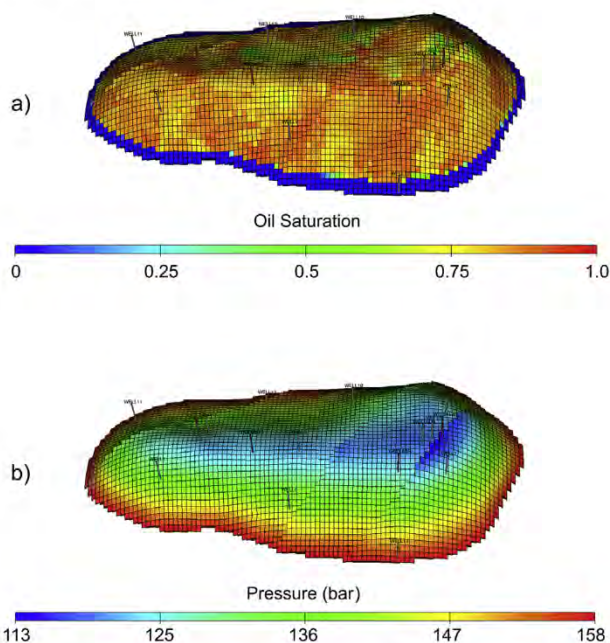


Fig. 20. (a) Initial oil saturation and (b) initial pressure distribution in the dynamic model.

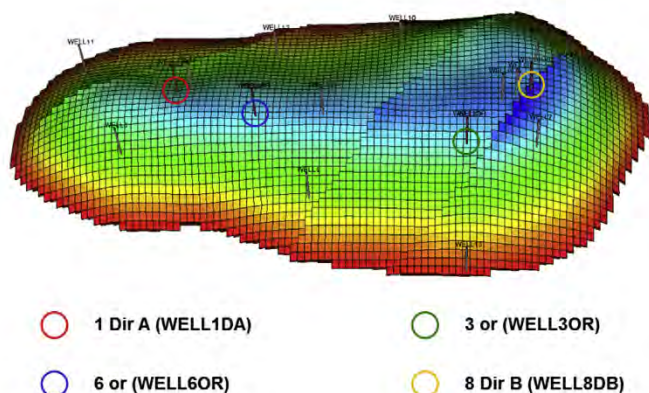


Fig. 21. Position of the active wells in the forecast phase.

each parameter on final results, namely the volume of hydrocarbon in place and expected final recovery. We described how data from geophysical interpretation and well log analysis can be used to account for both geological and petrophysical uncertainties. In the case of carbonate reservoirs, discrete fracture network (DFN) data can be taken from the combined interpretation of seismic and log data and assist in a reliable distribution of (micro) fracture petrophysical properties (Der-showitz et al., 1998; Karatolov et al., 2017). In our case, DFN data was used to define highly fractured areas and assign appropriate petrophysical values. In particular, permeability was defined by jointly evaluating well data, laboratory data, empirical relations, structural analysis and the DFN property and reflected the contribution of both the matrix and the fracture system. A similar approach was also followed for the data from geophysical interpretation, such as the attribute maps which can be easily transformed into 3D properties and then used in the analysis. The evaluation of the entire set of uncertain parameters was performed through the analysis of the histogram expressing the range of variation of the volume of oil originally in place.

After the volumetric evaluations, the results of the static modelling phase were transferred into a 3D numerical fluid-dynamic simulator to evaluate the propagation of the uncertainties associated to the input data

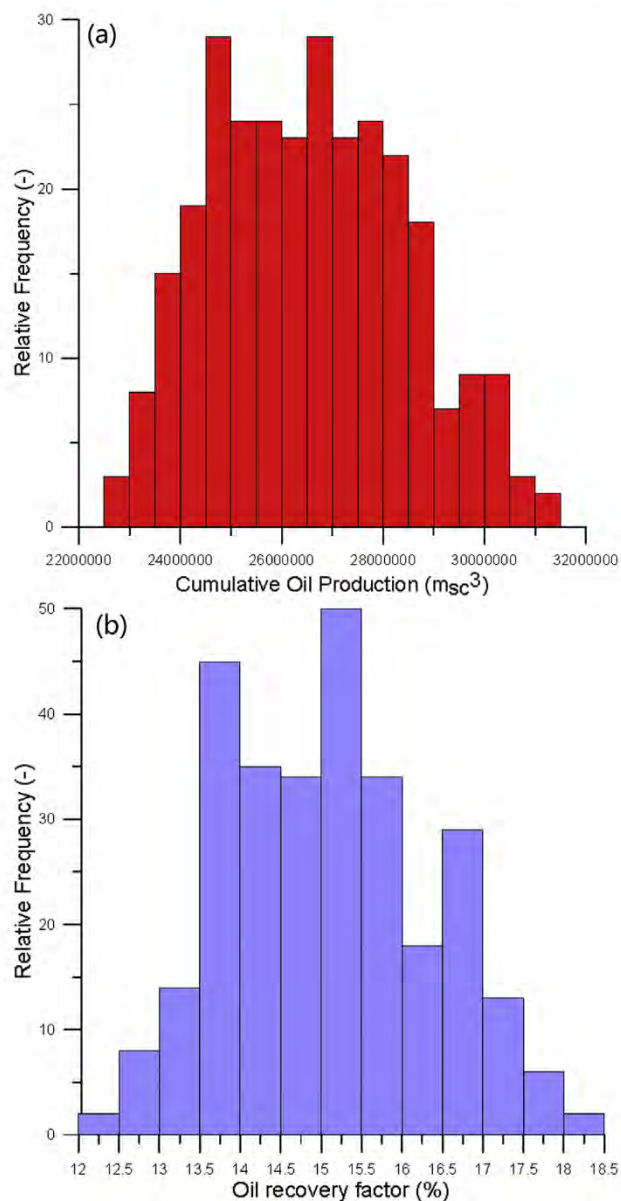


Fig. 22. (a) Cumulative oil production histogram and (b) Oil recovery factor histogram @12 years based on 300 dynamic simulations.

down to the final results and, specifically, to assess the dynamic response of the reservoir following a selected development plan. A single porosity approach was implemented in the dynamic model after verifying that the dynamic behavior of the reservoir could be adequately described as a system governed by a single equivalent porous medium comprising both matrix and fractures.

Results of the dynamic risk analysis allowed the statistical evaluation of the expected recoverable reserves and final recovery factors, by taking into account the uncertainties in the petrophysical characterization of the reservoir and providing a confidence range on the expected recoverable reserves and final recovery factors.

The overall risk analysis approach discussed in this paper is of general validity and can find application in various steps during the lifetime of a reservoir. Changes in the development strategy and/or the number, location and type of producing wells can be incorporated in the workflow so as to perform a statistically representative number of simulation runs and investigate the range of uncertainties according to possible future field operations. Thus, the described methodology can be used as a guideline for the optimization of the future reservoir development, by

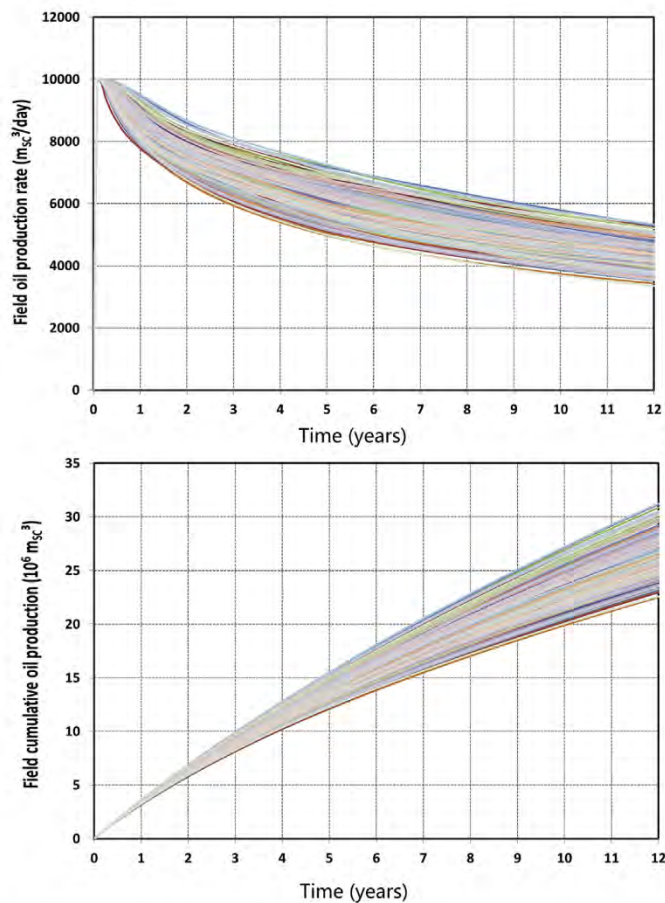


Fig. 23. Evolution in time of the (a) Field oil production rate and (b) Cumulative oil production based on 300 dynamic simulations.

assessing risks and optimizing interventions and investments. Furthermore, the workflow proposed in this work ensures and enhances the “integrated approach”, which is crucial for any reservoir study. It can be used as a reference for the participating members of a project since it allows the combination of any type of input data with their corresponding uncertainties, regardless of the uncertainty’s type and origin. Eventually, it can become part of educational training systems for young geoscientists and engineers (Verga et al., 2012) since a well-constructed workflow is the backbone of any reservoir study requiring true data integration and confidence analysis on the obtained results.

#### Declaration of competing interest

The authors declare that they have no known competing financial interests or personal relationships that could have appeared to influence the work reported in this paper.

#### Acknowledgements

The authors are grateful to Prof. Francesca Verga for fruitful discussions and an anonymous reviewer for his constructive comments and suggestions that significantly improved the manuscript.

#### References

Al-Qassab, H.M., Fitzmaurice, J., Al-Ali, Z.A., Al-Khalifa, M.A., Aktas, G.A., Glover, P.W., 2000. Cross-Discipline Integration in Reservoir Modeling: the Impact on Fluid Flow Simulation and Reservoir Management. Society of Petroleum Engineers, SPE-62902-MS. <https://doi.org/10.2118/62902-MS>.

Bahorich, M., Farmer, S., 1995. Seismic discontinuity for faults and stratigraphic features: the coherence cube. *Lead. Edge* 14, 1053–1058.

Bai, M., Elsworth, D., Roegiers, J.-C., 1993. Multiporosity/multipermeability approach to the simulation of naturally fractured reservoirs. *Water Resour. Res.* 29 (6), 1621–1633.

Baker, L.E., 1998. Three-Phase Relative Permeability Correlations. Society of Petroleum Engineers, SPE-17369-MS. <https://doi.org/10.2118/17369-MS>.

Barale, L., Bertok, C., d’Atri, A., Domini, G., Martire, L., Piana, F., 2013. Hydrothermal dolomitization of the carbonate jurassic succession in the provençal and subbriançonnais domains, maritime alps, north-western Italy. *Compt. Rendus Geosci.* 345 (1), 47–53.

Benetatos, C., Viberti, D., 2010. Fully integrated hydrocarbon reservoir studies: myth or reality? *Am. J. Appl. Sci.* 7 (11), 1477–1486.

Bloch, G., El Deeb, M., Badaam, H., Cailly, F., Iecante, G., Meunier, A., 2003. Seismic Facies Analysis for Fracture Detection : a Powerful Technique. Society of Petroleum Engineers, SPE-81526-MS. <https://doi.org/10.2118/81526-MS>.

Buckles, R.S., 1965. Correlating and Averaging Connate Water Saturation Data. Society of Petroleum Engineers, PETSOC-65-01-07. <https://doi.org/10.2118/65-01-07>.

Carter, R.D., Tracy, G.W., 1960. An Improved Method for Calculating Water Influx. Society of Petroleum Engineers, SPE-1626-G.

Choi, J.-H., Edwards, P., Ko, K., Kim, Y.-S., 2016. Definition and classification of fault damage zones: a review and a new methodological approach. *Earth Sci. Rev.* 152, 70–87.

Cipolla, Craig L., Lolon, Elyezer P., Erdle, Jim C., Rubin, Barry, 2010. Reservoir Modeling in Shale-Gas Reservoirs. Society of Petroleum Engineers, SPE-125530-PA. <https://doi.org/10.2118/125530-PA>.

Cosentino, L., 2001. Integrated Reservoir Studies. Institut Français du Pétrole Publications. Editions Technip ed., Paris, 310 pp.

Craft, B.C., Hawkins, M., 1991. Applied Petroleum Reservoir Engineering, second ed. Prentice-Hall Inc., Englewood Cliffs. 448 pp.

Davis, G.R., Smith, L.B., 2006. Structurally controlled hydrothermal dolomite reservoir facies: an overview. *AAPG (Am. Assoc. Pet. Geol.) Bull.* 90 (11), 1641–1690.

Dershowitz, B., LaPointe, P., Eiben, T., Wei, L., 1998. Integration of Discrete Feature Network Methods with Conventional Simulator Approaches. Society of Petroleum Engineers, SPE-49069-MS. <https://doi.org/10.2118/49069-MS>.

Du, C., Zhang, X., Melton, B., Fullilove, D., Suliman, B., Gowelly, S., Grant, D., Calvez, J., 2009. A Workflow for Integrated Barnett Shale Gas Reservoir Modeling and Simulation. Society of Petroleum Engineers, SPE-122934-MS. <https://doi.org/10.2118/122934-MS>.

Faulkner, D.R., Jackson, C.A.L., Lunn, R.J., Schlische, R.W., Shipton, Z.K., Wibberley, C.A.J., Withjack, M.O., 2010. A review of recent developments concerning the structure, mechanics and fluid flow properties of fault zones. *J. Struct. Geol.* 32, 1557–1575.

Gersztenkorn, A., Marfurt, K.J., 1999. Eigenstructure-based coherence computations as an aid to 3-D structural and stratigraphic mapping. *Geophysics* 64 (5), 1468–1479.

Guerreiro, L., Silva, A.C., Alcobia, V., Soares, A., 2000. Integrated Reservoir Characterisation of a Fractured Carbonate Reservoir. Society of Petroleum Engineers, SPE-58995-MS. <https://doi.org/10.2118/58995-MS>.

Harris, P.M., 1985. Depositional environments of carbonate platforms. *Carbonate depositional environments, modern and ancient, Part 2. Colo. Sch. Mines Q.* 80 (4), 31–60.

Holmes, M., Holmes, A., Holmes, D., 2009. Relationship between porosity and water saturation: methodology to distinguish mobile from capillary bound water. In: Adapted from Oral Presentation at AAPG Annual Convention, Denver, Colorado, June 7–10, 2009 AAPG National Meeting. [http://www.searchanddiscovery.com/documents/2009/110108holmes/ndx\\_holmes.pdf](http://www.searchanddiscovery.com/documents/2009/110108holmes/ndx_holmes.pdf).

Karatolov, N., Stefaniak, A., Vaughan, L., 2017. DFN Modeling Aided Reservoir Characterization. Society of Petroleum Engineers, SPE-188641-MS. <https://doi.org/10.2118/188641-MS>.

Labourdet, R., Meyer, A., Sudrie, M., Walgenwitz, F., Javaux, C., 2007. Nested Stochastic Simulation : a New Approach in Assessing Spatial Distribution of Carbonate Sedimentary Facies and Associated Diagenetic Overprints. Society of Petroleum Engineers SPE 111410-MS. <https://doi.org/10.2118/111410-MS>.

Labourdet, R., Hegre, J., Imbert, P., Insalaco, E., 2008. Reservoir-scale 3D Sedimentary Modelling: Approaches to Integrate Sedimentology into a Reservoir Characterization Workflow, 309. Geological Society of London, Special Publications, pp. 75–85.

Langhorne Jr., B.S., Davies, G.R., 2006. Structurally controlled hydrothermal alteration of carbonate reservoirs: Introduction. *AAPG (Am. Assoc. Pet. Geol.) Bull.* 90 (11), 1635–1640.

Le Ravelac, M., Doligez, B., Lerat, O., 2014. Integrated Reservoir Characterization and Modelling. E-book, IFP Energies Nouvelles publication, Paris, France. <https://doi.org/10.2516/ifpen/2014001>.

Ma, Y. Zee, Gomez, E., Luneau, B., Iwere, F., Young, T.J., Cox, D.L., 2011. Integrated reservoir modeling of a pinedale tight-gas reservoir in the greater green river basin, Wyoming. In: Ma, Y.Z., La Pointe, P.R. (Eds.), *Uncertainty Analysis and Reservoir Modeling: AAPG Memoir*, 96, pp. 89–106.

Marfurt, K.J., Kirilin, R.L., Farmer, S.L., Bahorich, M.S., 1998. 3-D seismic attributes using a semblance-based coherency algorithm. *Geophysics* 63, 1150–1165.

Marfurt, K.J., Sudhaker, V., Gersztenkorn, A., Crawford, K.D., Nissen, S.E., 1999. Coherency calculations in the presence of structural dip. *Geophysics* 64, 104–111.

Morrow, D., 2016. 2016. Hydrothermal dolomitization paradigms and the manetoe dolomite: are all HTDs Fault-related?. In: Oral Presentation (#51302) Given at AAPG 2016 Annual Convention and Exhibition, Calgary, Alberta, Canada, pp. 19–22. June.

Moscariello, A., 2016. Reservoir geo-modeling and uncertainty management in the context of geo-energy projects. *Swiss Bull. fürangewandte Geol.* 21 (1), 29–43.

Ouenes, A., Hartley, L.J., 2000. Integrated Fractured Reservoir Modeling Using Both Discrete and Continuum Approaches. Society of Petroleum Engineers, SPE-62939-MS. <https://doi.org/10.2118/62939-MS>.

- Quintana Saalfeld, R., Von Hohendorff Filho, J.C., Schiozer, D.J., 2016. Simulation of naturally fractured reservoirs using single-porosity equivalent models. In: Avila, Suzana Moreira (Ed.), Proceedings of the XXXVII Iberian Latin-American Congress of Computational Methods in Engineering CILAMCE 2016. ABMEC, Brasilia, DF, Brazil. November 6-9, 2016.
- Sarg, J.F., Markello, J.R., Weber, L.J., 1999. The second order cycle, carbonate platform growth, and reservoir, source, and trap prediction. In: Harris, P.M., Saller, J.A., Simo, J.A. (Eds.), Advances in Carbonate Sequence Stratigraphy: Application to Reservoirs, Outcrops, and Models, 63. SEPM Special publication, pp. 11–34.
- Schlager, W., 2007. Carbonate Sedimentology and Sequence Stratigraphy. SEPM Society for Sedimentary Geology, p. 200.
- Senel, O., Will, R., Butsch, R.J., 2014. Integrated reservoir modeling at the Illinois basin – decatur project. Greenhouse. Gases. Sci. Technol. 4, 662–684.
- Shao, Y., Zheng, A., He, Y., Xiao, K., 2011. 3D geological modeling and its application under complex geological conditions. Procedia Eng. 12, 41–46.
- Teutsch, G., 1993. An extended double-porosity concept as a practical modeling approach for a karstified terrain. Hydrogeological Processes in Karst Terranes. In: Proceedings of the Antalya Symposium and Field Seminar, October 1990. IAHS, Wallingford, UK, pp. 281–292.
- Tucker, M.E., Wright, V.P., 2009. Carbonate Sedimentology, first ed. Wiley-Blackwell, p. 496.
- Verga, F., Benetatos, C., Sacchi, Q., Carta, R., 2012. Development of a petroleum knowledge tutorial system for university and corporate training. Pet. Sci. 9 (1), 110–120.
- Vogel, T., Gerke, H.H., Zhang, R., Van Genuchten, M.T., 2000. Modeling flow and transport in a two-dimensional dual-permeability system with spatial variable hydraulic properties. J. Hydrol. 238, 78–89.
- Warren, J., 2000. Dolomite: occurrence, evolution and economically important associations. Earth Sci. Rev. 52, 1–8.
- Worthington, P.F., Cosentino, L., 2005. The Role of Cut-Offs in Integrated Reservoir Studies. Society of Petroleum Engineers, SPE-84387-PA. <https://doi.org/10.2118/84387-PA>.